JGR Biogeosciences

RESEARCH ARTICLE
10.1029/2021JG006673

Probability Distributions of Radiocarbon in Open Linear Compartmental Systems at Steady-State

Ingrid Chanca[1,2], Susan Trumbore[1], Kita Macario[2], and Carlos A. Sierra[1,3]

[1]Max-Planck-Institut für Biogeochemie, Jena, Germany, [2]Laboratório de Radiocarbono, Instituto de Física, Universidade Federal Fluminense, Niterói, Brazil, [3]Department of Ecology, Swedish University of Agricultural Sciences, Uppsala, Sweden

Key Points:

- Probability distributions of radiocarbon in ecosystem compartments can be derived from carbon age distributions
- The shape of these distributions vary according to the speed of carbon cycling and the year of observation
- Probability distributions of radiocarbon provide insights to study carbon dynamics and to interpret radiocarbon data

Supporting Information:

Supporting Information may be found in the online version of this article.

Correspondence to:

I. Chanca,
ichanca@bgc-jena.mpg.de

Citation:

Chanca, I., Trumbore, S., Macario, K., & Sierra, C. A. (2022). Probability distributions of radiocarbon in open linear compartmental systems at steady-state. *Journal of Geophysical Research: Biogeosciences*, *127*, e2021JG006673. https://doi.org/10.1029/2021JG006673

Received 14 OCT 2021
Accepted 8 MAR 2022

Abstract Radiocarbon (^{14}C) is commonly used as a tracer of the carbon cycle to determine how fast carbon moves between different reservoirs such as plants, soils, rivers, or oceans. However such studies mostly emphasize the mean value (as $\Delta^{14}C$) of an unknown probability distribution. We introduce a novel algorithm to compute $\Delta^{14}C$ distributions from knowledge of the age distribution of carbon in linear compartmental systems at steady-state. Our results demonstrate that the shape of the distributions might differ according to the speed of cycling of ecosystem compartments and their connectivity within the system, and might contain multiple peaks and long tails. The distributions are also sensitive to the variations of $\Delta^{14}C$ in the atmosphere over time, as influenced by the counteracting anthropogenic effects of fossil-fuel emissions (^{14}C-free) and nuclear weapons testing (excess ^{14}C). Lastly, we discuss insights that such distributions can offer for sampling and design of experiments aiming to capture the precise variance of $\Delta^{14}C$ values present in the multi-compartmental ecosystems.

Plain Language Summary Radiocarbon (^{14}C) is a radioactive isotope of carbon prominent in environmental sciences for tracing the dynamics of ecosystems, especially as recent changes in atmospheric radiocarbon allow tracking excess ^{14}C created by nuclear weapons testing in the atmosphere on timescales shorter than what can be determined using radioactive decay. For climate change mitigation, a crucial uncertainty is the time carbon captured through photosynthesis spends in ecosystems before being released. For this purpose, radiocarbon can be valuable as a biological tracer; however, it is necessary to accurately link the real age of carbon and its radiocarbon age, as they usually differ. Forests and soils are open systems, connecting components with intrinsically different cycling timescales, so that the mean age comes from an age distribution that is usually unknown. Here, we developed an algorithm to compute the ^{14}C contents for models consisting of multiple interconnected carbon pools. Our approach offers more accurate estimations of the mean ^{14}C content of the system and computations of the distribution of ^{14}C within the system at different points in time. Results obtained from this method can provide additional insights on the dynamics of the carbon cycle in multiple compartments, and can help to better interpret observations.

1. Introduction

Radiocarbon (^{14}C) is a valuable tool for studying dynamical processes in living systems. In particular, radiocarbon produced by nuclear bomb tests in the 1960s has been used in many contexts as a tracer for the dynamics of carbon in different compartments of the global carbon cycle, including the atmosphere, the terrestrial biosphere, and the oceans (Goudriaan, 1992; Jain et al., 1997; Levin et al., 2010; Naegler et al., 2006; Randerson et al., 2002). As a biological tracer, radiocarbon can be used to infer rates of carbon cycling in specific compartments, and to infer transfers among interconnected compartments. Therefore, radiocarbon is used as a diagnostic metric to assess the performance of models of the carbon cycle (Graven et al., 2017), and new data sets are now emerging to incorporate radiocarbon in model benchmarking (Lawrence et al., 2020).

Carbon cycling in biological systems can be represented using a particular class of mathematical models called compartmental systems (Sierra et al., 2018). As carbon enters a system such as the terrestrial biosphere, it is stored and transferred among a network of interconnected compartments such as foliage, wood, roots, soils, and other organisms. Compartmental systems represent the dynamics of carbon as it travels along the network of compartments (Rasmussen et al., 2016; Sierra et al., 2018), and provide information about the time carbon spends in particular compartments and the entire system (Rasmussen et al., 2016; Sierra et al., 2017). Although

there seems to be a direct relation between the time carbon spends in a compartmental system and its radiocarbon dynamics, few studies relate both concepts.

An open compartmental system contains inflows and outflows different from zero (Jacquez & Simon, 1993). Timescales in open compartmental systems are usually characterized by the concepts of *age* and *transit time* (Bolin & Rodhe, 1973; Rasmussen et al., 2016; Sierra et al., 2017). In open systems such as the biosphere, the incorporation and release of carbon occurs continuously, and it is possible to define the concept of *age* as the time elapsed since carbon enters the compartmental system until a generic time. The *transit time* can be defined as the time the carbon needs to travel through the entire system, that is, the time elapsed between carbon entry until its exit. In order to estimate these time metrics from ^{14}C measurements, a model linking both carbon and radiocarbon dynamics is required. Thompson and Randerson (1999) have used impulse response functions from compartmental models to obtain ages, transit times, and time-dependent radiocarbon dynamics. However, this approach is computationally expensive and can introduce numerical errors if simulations are not long enough to cover the dynamics of slow cycling pools.

Explicit formulas for age and transit time distributions in compartmental systems have been recently developed (Metzler & Sierra, 2018). These formulas do not introduce numerical errors and can describe entire age distributions of carbon for specific pools and for the entire compartmental system. These age distributions suggest that radiocarbon in compartmental systems may consist of a mix of different values, that is, compartments could be described in terms of radiocarbon distributions that relate the relative proportion of carbon with a particular radiocarbon value. However, until now, radiocarbon is reported and modeled as a single quantity, rather than the mean of an underlying distribution.

Knowledge of the distribution of the isotopic ratio between ^{14}C to ^{12}C in a compartmental system might give important insights on the model structure that better fits existing data. For example, by comparing the signature of radiocarbon in the pools and their outfluxes, we get insights into the size of the compartmental model that better describes ecosystem dynamics (Sierra et al., 2017). Further, empirical knowledge of the radiocarbon distribution of a particular system can play a significant role in determining the most appropriate model to describe a system.

Model-data comparisons using radiocarbon are made more complex by the fact that the quantity of ^{14}C in the atmosphere is continuously changing. This is particularly important after the 1960s when nuclear bomb tests liberated large amounts of thermal neutrons to the atmosphere, contributing to the formation of radiocarbon (bomb or excess ^{14}C). In addition, large quantities of fossil-fuel derived carbon (^{14}C-free) have been emitted to the atmosphere since the beginning of the Industrial Revolution, diluting the atmospheric radiocarbon signal and producing a fast decline of the radiocarbon isotopic ratio in recent years (Graven et al., 2017). Therefore, we would expect a different radiocarbon distribution for every year in a compartmental system.

However, most studies have focused on estimating the mean isotopic ratio of ^{14}C to ^{12}C in order to evaluate carbon ages and transit times, ignoring its potential underlying distribution. As a tracer, the entire distribution of radiocarbon values are expected to change over time even if the compartmental system is in equilibrium. Thus, obtaining a simple and accurate method to estimate radiocarbon distributions as a function of time (e.g., the year of observation or sample collection) is of great interest for experimental and modeling studies. Therefore, the main objective of this manuscript is to introduce a method to obtain distributions of radiocarbon in compartmental systems at steady-state. In particular, we ask the following research questions: (a) How do distributions of radiocarbon in terrestrial compartments change over time as a consequence of changes in atmospheric radiocarbon? (b) How do empirical data compare to these conceptual radiocarbon distributions? (c) What insights can these distributions provide for experimental and sampling design for improving model-data comparisons by capturing the entire variability of $\Delta^{14}C$ values?

The manuscript is organized as follows: First, we provide the necessary theoretical background to obtain age and transit time distributions from compartmental systems. Second, we describe an algorithm that computes radiocarbon distributions for particular years using an age or a transit time distribution of carbon and an atmospheric radiocarbon curve. Third, we present an application of our algorithm to three compartmental systems addressing the research questions above. Finally, we discuss our results in the context of applications to any general compartmental model and potential new insights from our approach.

2. Age and Transit Time Distributions in Compartmental Systems

2.1. Compartmental Systems

Compartmental systems describe the temporal dynamics of matter as it travels through a network of compartments until its final release from the system. A set of compartments is translated mathematically as a set of linear or nonlinear ordinary differential equations, whose solutions are the amount of matter in each compartment at a certain time.

We will consider here linear autonomous compartmental systems, characterized by the mass of carbon at time t in m compartments as the vector $\boldsymbol{x}(t) \in \mathbb{R}^m$. Additionally, the compartments of the systems considered here are assumed well mixed, which implies that all carbon atoms inside a compartment have the same probability of being transferred to other compartments or to outside the system (Anderson, 1983). This well-mixed property is linked to the fixed-rate at which mass is processed inside each compartment. For example, if a compartment i has a process rate k_i, all particles inside the compartment have the same probability of being removed from the compartment at this rate.

The mass of carbon in the compartments changes over time according to the following expression:

$$\frac{d\boldsymbol{x}(t)}{dt} = \dot{\boldsymbol{x}}(t) = \boldsymbol{u} + \mathbf{B}\,\boldsymbol{x}(t), \qquad \boldsymbol{x}(t=0) = \boldsymbol{x_0}, \tag{1}$$

where the constant vector $\boldsymbol{u}$ represents the inputs of carbon into the system, and the $m \times m$ compartmental matrix $\mathbf{B}$ contains constant values of the cycling rates of the compartments in its diagonal entries, while the off-diagonal entries consist of the constant transfer rates among them. In particular, the compartmental matrix in most ecosystem carbon models has an internal structure reflecting transfers between the components (coefficients $\alpha_{i,j}$, representing the proportion of C transferred from compartment j to compartment i) and cycling rates k_i reflecting assumptions of first-order kinetics of loss (at rate k_i) from any given compartment:

$$\mathbf{B} = \begin{pmatrix} -k_1 & \alpha_{1,2}k_2 & \cdots & \alpha_{1,m}k_m \\ \alpha_{2,1}k_1 & -k_2 & \cdots & \alpha_{2,m}k_m \\ \vdots & \vdots & \ddots & \vdots \\ \alpha_{m,1}k_1 & \alpha_{m,2}k_2 & \cdots & -k_m \end{pmatrix}. \tag{2}$$

This matrix contains information on the dynamics, structure, and size of a compartmental model. The outflux of carbon from the system can also be obtained from this matrix by summing all column elements; that is, the outputs from a pool that are not transferred to other pools are assumed to leave the compartmental system.

The information of the amount of carbon entering the system to be partitioned among the compartments is contained in the input vector:

$$\boldsymbol{u} = \begin{pmatrix} u_1 \\ u_2 \\ \vdots \\ u_m \end{pmatrix}. \tag{3}$$

Linear autonomous systems of the form of Equation 1 have an equilibrium point or steady-state solution $\boldsymbol{x}^*$ given by:

$$\boldsymbol{x}^* = -\mathbf{B}^{-1}\,\boldsymbol{u}, \tag{4}$$

where the mass of the compartments do not change over time, and inputs are equal to outputs for all compartments.

2.2. Age Distributions

We define age τ in a compartmental system as the time elapsed between the time of carbon entry until some generic time (Sierra et al., 2017). For a time-independent system in steady-state, a probability distribution of ages of carbon in the compartments can be obtained using stochastic methods. According to Metzler and Sierra (2018), the vector of age densities for the compartments (denoted by $\boldsymbol{f}_a(\tau)$) can be obtained as:

$$\boldsymbol{f}_a(\tau) = (\mathbf{X}^*)^{-1} e^{\tau \mathbf{B}} \boldsymbol{u} \tag{5}$$

where $\mathbf{X}^* = \text{diag}\left(x_1^*, x_2^*, \ldots, x_m^*\right)$ is the diagonal matrix with the steady-state vector of carbon stocks as components, and $e^{\tau\ \mathbf{B}}$ is the matrix exponential.

For the whole system (denoted by the function with capital A, $f_A(\tau)$), the age distribution is given by:

$$f_A(\tau) = -\mathbf{1}^\intercal \mathbf{B} e^{\tau \mathbf{B}} \frac{\boldsymbol{x}^*}{\|\boldsymbol{x}^*\|}, \tag{6}$$

where $\|\boldsymbol{x}^*\| := \sum_{j=1}^{m} |\boldsymbol{x}^*|$ is the 1-norm of the steady-state solution and represents the sum of the masses in the vector.

2.3. Transit Time Distributions

We define transit time as the time elapsed since carbon enters the compartmental system until it leaves the boundaries of the system (Sierra et al., 2017). The transit time is equivalent, therefore, to the age of the outflux. Metzler and Sierra (2018) also provide an explicit formula to obtain the transit time density distribution for a time-independent system at steady-state as:

$$f_{TT}(\tau) = -\mathbf{1}^\intercal \mathbf{B} e^{\tau \mathbf{B}} \frac{\boldsymbol{u}}{\|\boldsymbol{u}\|}. \tag{7}$$

The age and transit time distributions are densities and they integrate to 1:

$$\int_0^\infty f_A(\tau)\, d\tau = \int_0^\infty f_{TT}(\tau)\, d\tau = 1. \tag{8}$$

The derivation of these Equations 5–7 is based on the idea that a deterministic compartmental system of differential equations can be expressed as a continuous-time Markov chain (Metzler & Sierra, 2018). This perspective, allows us to make inferences about the total masses of carbon in a stochastic setting, with explicit formulas for the age of carbon atoms in the system (Azizi-Rad et al., 2021).

3. Methods

3.1. Radiocarbon Distributions From Age and Transit Time Distributions

We developed an algorithm to convert age and transit time distributions into distributions of radiocarbon expressed as $\Delta^{14}C$ for any given year of observation. We define $\Delta^{14}C$ as:

$$\Delta^{14}C = \left[F^{14}C e^{\lambda_C (1950-y)} - 1\right] \times 1000\ [‰] \tag{9}$$

where $F^{14}C$ is the Fraction Modern (A_{SN}/A_{ON}), that is, the sample ratio normalized to $\delta^{13}C$ by oxalic acid standard (OXII), λ_C is the updated ^{14}C decay constant (equals 1/8,267 [y^{-1}]), and y is the year of measurement.

The algorithm works in three main steps, (1) homogenization, (2) discretization, and (3) aggregation (Figure 1). We describe these three steps in detail in the sections below using mathematical notation for the system age distribution, but computations are similar for the transit time distribution, and the age distribution of individual compartments.

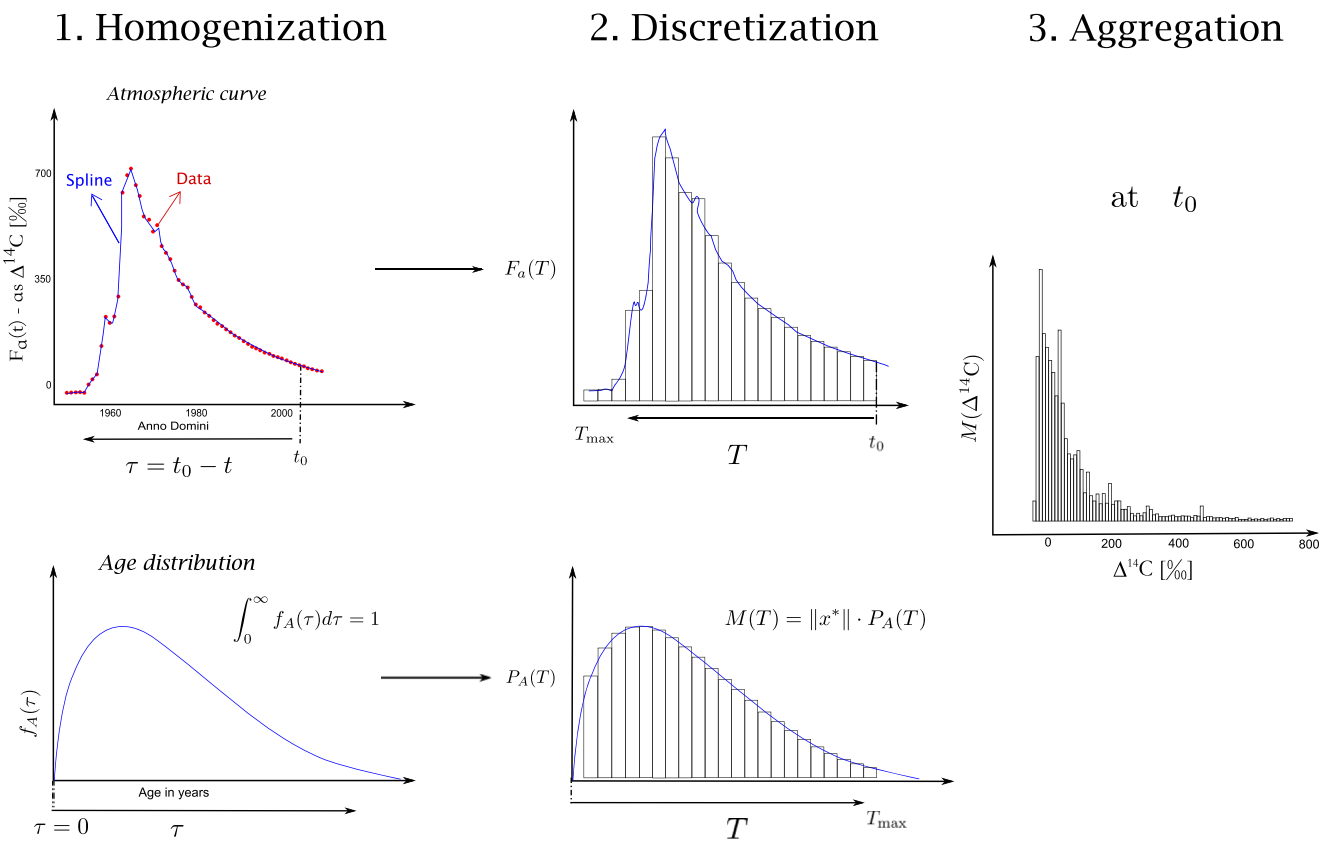

Figure 1. Graphical visualization of the three main steps for the computation of radiocarbon distributions in a compartmental system using an atmospheric radiocarbon curve of the carbon inputs to the systems, and the age distribution of carbon in a compartmental system. The homogenization step (1) consists of normalizing the times variables of the atmospheric curve, which is expressed in years of the calendar, and the age distributions, with ages in years. In the step 1, we also apply a spline interpolation to the atmospheric radiocarbon data set to make sure both curves—atmospheric radiocarbon and age distribution—have the same resolution h. In the discretization step (2) we divide the continuous curves into discrete intervals, where the masses of carbon will correspond to the probability densities obtained by the computation of the age distribution, multiplied by the steady-state solution of the compartmental system. Finally, in the aggregation (3) we subdivide the atmospheric radiocarbon curve into intervals with size of the final bin size of the bar-plots, that is, b, and sum the masses of carbon from the age distribution with the same $\Delta^{14}C$ value they would have in the atmosphere, independent of the age.

3.1.1. Homogenization of Input Data

The main inputs for the algorithm are an age distribution $f_A(\tau)$, and an atmospheric radiocarbon curve $F_a(t)$ that provides the $\Delta^{14}C$ value of atmospheric CO_2 for a calendar year t. To homogenize the time variable of both $f_A(\tau)$ and $F_a(t)$, we define the year of observation t_0, as the year of interest to produce the radiocarbon distribution. In this way, we have f_A and F_a in terms of the same independent variable.

Since we are interested in determining the radiocarbon values of material observed in the system at time t_0, we will look in the radiocarbon curve $-t$ years in the past to obtain the radiocarbon values in the system with an age τ. Therefore, atmospheric radiocarbon can be expressed as a function of age, that is, $F_a(t_0 - t) = F_a(\tau)$ (Figure 1). Now, both the system age distribution $f_A(\tau)$ and the atmospheric radiocarbon curve $F_a(\tau)$ are functions of the continuous variable τ that represents age since t_0.

Several atmospheric radiocarbon data sets can be found in the literature (Graven et al., 2017; Hogg et al., 2013, 2020; Hua et al., 2013, 2021; Levin & Kromer, 1997; Levin et al., 1980, 2010; Reimer et al., 2013, 2020). Also, forecasts of radiocarbon content in the atmosphere can be found in the recent literature (Graven, 2015; Sierra, 2018). However, these atmospheric radiocarbon data sets do not necessarily have the same resolution in time. Some of them provide predictions or data at an annual or four-monthly time step, while in other data sets, some ranges are spaced by decades. To homogenize the resolution of the $\Delta^{14}C$ and to transform these radiocarbon data sets into a continuous function of τ, we use a cubic spline interpolation to obtain $\Delta^{14}C$ values for any value of τ. After this

step, $F_a(\tau)$ can be computed until the last available date in the chosen atmospheric radiocarbon data set, covered by the range where $f_A(\tau)$ is computed, that is, for any value of $\tau \in [0, \infty)$.

3.1.2. Discretization

Although we have now the age distribution and the radiocarbon data as continuous functions of age, we need to discretize these functions in intervals of size h. The reason for this discretization is that the probability density function of age $f_A(\tau)$ is a measure of the relative likelihood of an infinitesimal amount of mass having an age τ. But ultimately, we are interested in the probability that a small mass has certain radiocarbon distribution. Therefore, we need to discretize the probability density function to a probability mass function along a discrete variable $T \in [0, T_{\max}]$. The new discrete probability function of ages can be defined as:

$$P_A(\tau \leq T \leq \tau + h) = \int_{\tau}^{\tau+h} f_A(\tau) d\tau. \tag{10}$$

From this probability function, we can compute the proportion of total mass in the system with an age T as:

$$M(T) = \|\boldsymbol{x}^*\| \cdot P_A(T), \tag{11}$$

where

$$\begin{aligned} \sum_{T=0}^{T_{\max}} P_A(T) &\approx 1, \\ \sum_{T=0}^{T_{\max}} M(T) &\approx \|\boldsymbol{x}^*\|. \end{aligned} \tag{12}$$

Equation 12 implies that there is an approximation error by discretizing the continuous density function to a finite set of discrete intervals. This approximation error can be minimized by decreasing the size of the intervals h and extending $T_{\max}$ as far as possible.

Once we discretize $f_A(\tau)$ to $P_A(T)$ and obtain discrete proportions of mass with certain age $M(T)$, we proceed to discretize the atmospheric radiocarbon curve with respect to the same discrete interval of ages $T \in [0, T_{\max}]$. This is simply done by computing $F_a(\tau = T)$, which makes the assumption that within each interval $[\tau, \tau + h]$, the atmospheric radiocarbon value is equal to $F_a(\tau)$.

3.1.3. Aggregation

Now we are ready to combine the distribution of mass in the system at discrete age intervals with the atmospheric radiocarbon curve. To do so, we first subdivide the $\Delta^{14}C$ axis of the radiocarbon curve into equally spaced bins (b); for each bin b we take the corresponding radiocarbon content $F_a(T)$ and corresponding intervals of $T \in [0, T_{\max}]$, matching them to the respective values of mass $M(T)$ in the age distribution of carbon. Then, we sum all the masses within the same $\Delta^{14}C$ values (see Figure S1 in Supporting Information S1 for a better understanding of the aggregation step). The result can be organized as the amount of carbon mass in discrete intervals of $\Delta^{14}C$; that is, $M(\Delta^{14}C) = M(F_a(T))$.

We implemented these three steps in the R programming language, and used the package SoilR (Sierra, Müller, & Trumbore, 2012) to obtain the age distribution of the pools, the whole system, and the output flux (equivalent to the transit time) based on Equations 5–7. The versions used here were R version 4.0.3 and SoilR version 1.1 (Sierra et al., 2014). The link to access the R scripts with the algorithm functions and model results is provided in the *data availability statement*.

Since atmospheric ^{14}C concentration for the past 55,000 yr is mainly empirically known, generating the radiocarbon curves, we could easily convert age into atmospheric $\Delta^{14}C$. By matching the $\Delta^{14}C$-based-on-age values with the previously estimated densities, we built barplots, gaining insight into the radiocarbon distributions for the models studied in this work. In the algorithm we defined four functions: *PoolRDC*, *SystemRDC*, *TTRDC*, and *C14hist*. The first three functions take the densities outputs, that is, the carbon contents discretized by age, from

built-in SoilR functions, such as *transitTime* and *systemAge*. The densities are subset to build bins through the *C14hist* function. The logical statements used to construct the bins are based on the atmospheric $\Delta^{14}C$ data and according to user-defined bin size b. This structure allows one to plot histogram-like graphs, where the height of the bars represent the amount of carbon mass with corresponding $\Delta^{14}C$ values. Thus, our algorithm starts with a compartmental matrix, an input vector and a radiocarbon calibration curve, and returns an object containing masses of C and their matching decay-corrected $\Delta^{14}C$ values, estimated for any given year of observation. The match is done by assuming that $\tau = 0$ (age equals zero) at the year of observation t_0. This means that the input radiocarbon signal in past years will correspond to the $\Delta^{14}C$ signal of the atmosphere of those years corrected for the radioactive decay of ^{14}C (average lifetime of 8,267 yr, i.e., half-life of 5,730 yr) according to the age of the pool, system or outflux.

Besides the radiocarbon distributions for pools, whole system and output flux, one can also compute the expected value of $\Delta^{14}C$ from these distributions in any given year of observation. This is done by computing the mean of $\Delta^{14}C$ weighted by the amount of carbon in $\Delta^{14}C$ bins of size b. The standard deviation (sd) of the distribution is obtained as the square root of the difference between the square of the expected value and the expected value of the squares of $\Delta^{14}C$ values.

3.2. Carbon Cycle Models

Our approach can be used to obtain radiocarbon distributions for linear compartmental models of any size representing carbon cycling processes at different scales and for different biological systems. We discuss here the probability distributions of radiocarbon obtained for three different carbon cycle models. Despite the method described throughout this work may not be limited to these examples, the approach is particularly useful for interpretation of radiocarbon measurements in ecosystems in the future. Nevertheless further applications might include carbon dynamics in aquatic systems, molecular transformations of carbon in organisms, among others.

In the following sections, we focus on a model that represents the dynamics of soil organic carbon in a temperate forest, which we call here the Harvard Forest Soil (HFS) model. In the appendix, we describe two other carbon models, hereafter called Porce model and Emanuel model. The Porce model represents the carbon cycle of a tropical forest in the Porce region (Colombia) through seven interconnected compartments (Sierra et al., 2021). The Emanuel model describes the global carbon cycle through a 5-box model (Emanuel et al., 1981).

The pools of the HFS model were operationally defined, which means they were based on methods to separate organic matter performed on samples from the Harvard Forest in Massachusetts, USA (Gaudinski et al., 2000; Sierra, Trumbore, et al., 2012). Soil samples collected in O-horizon, corresponding to 0–8 cm depth, and A-horizon (8–15 cm depth) were separated into seven soil fractions corresponding later to each of the compartments of the model (Figure 2); one pool corresponds to *dead roots* x_1. Pools x_2, x_3, and x_4 correspond, respectively, to fractions from the O-horizon here called *Oi*, *Oe/a L*, and *Oe/a H*. We keep the pool names given in Gaudinski et al. (2000) and Sierra, Trumbore, et al. (2012), but these fractions are equivalent to leaf litter (*Oi* fraction), recognizable root litter (*Oe/a L* fraction), and humified fraction, that is, organic matter that has been transformed by microbial action (*Oe/a H*). Pools x_5, x_6, and x_7 correspond, respectively, to fractions from the A-horizon here called *A, LF* (>80 μm), *A, LF* (<80 μm), and *mineral associated*. The A-horizon pools were fractionated by density (1 g cm^{-3}), with the low-density portion being further subdivided by sieving into recognizable leaf larger than 80 μm (*A, LF* (>80 μm) fraction, pool x_5) and smaller than 80 μm (*A, LF* (<80 μm) fraction, pool x_6). Details about the methods employed to fractionate the samples can be found in Gaudinski et al. (2000).

The HFS model was built by fitting empirical radiocarbon data from the above described soil fractions. Details about the use of the data to build the compartmental model are presented in Sierra, Trumbore, et al. (2012). For the same sites, independent data (i.e., data not used for estimating the compartmental matrix) are available (Sierra, Trumbore, et al., 2012). The independent data used in this work consists of $\Delta^{14}C$ measurements on total soil CO_2 efflux collected between 1996 and 2010 (with exception for the year 2005). We used these data to compare the representativity of the mean $\Delta^{14}C$ measurements to the expected $\Delta^{14}C$ values obtained through our algorithm. In the results, we present the probability distributions of radiocarbon for the years 1996, 1998, 2002, and 2008. The number of samples measured corresponding to the respective years was n = 12, 28, 23, and 10.

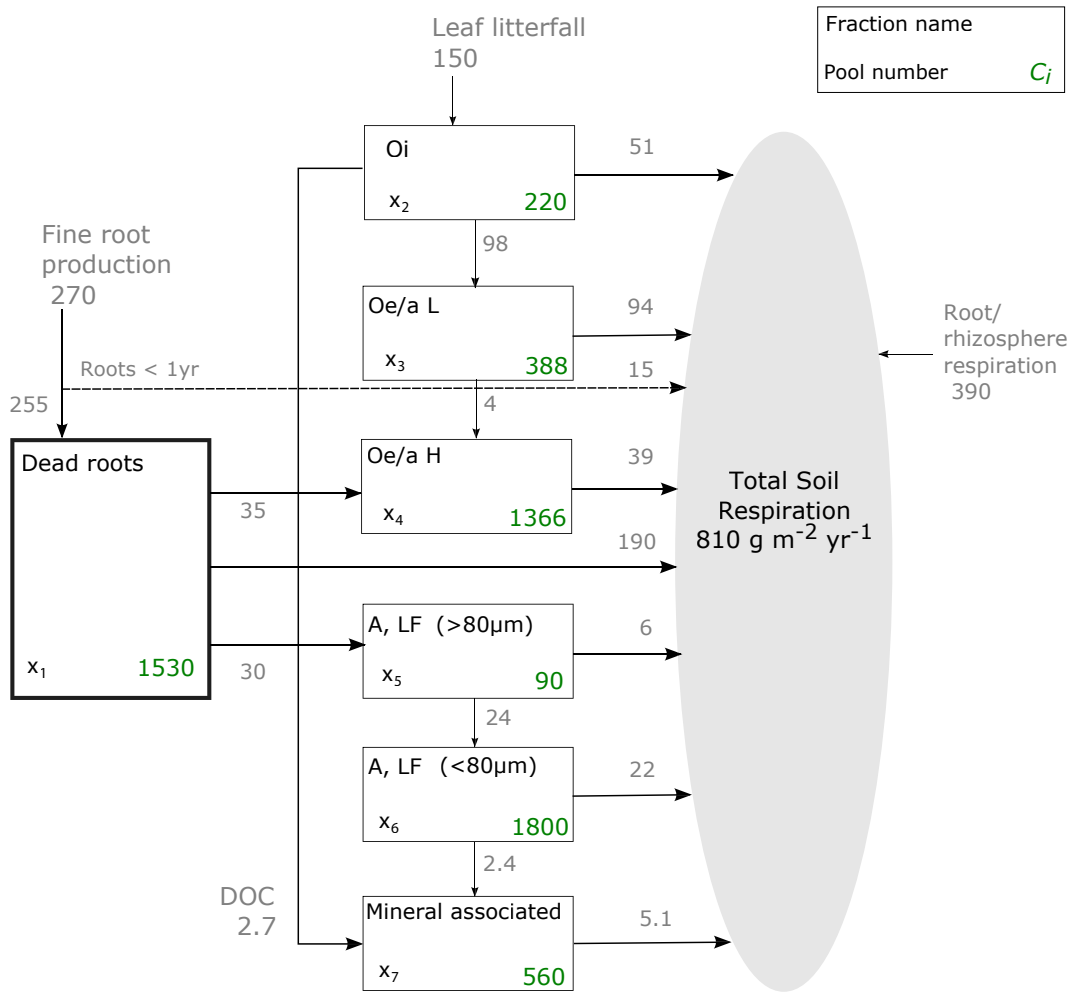

Figure 2. Scheme of Harvard Forest soil model stocks (C_i) and fluxes among compartments (adapted from Sierra, Trumbore, et al., 2012). All the fluxes are in units of gC m^{-2} yr^{-1} and stocks in gC m^{-2}. Pool x_1 corresponds to *dead roots*; in the O-horizon we have pools x_2: *Oi* (leaf litter), x_3: *Oe/a L* (recognizable root litter), and x_4: *Oe/a H* (humidified OM). In the A-horizon, we have pools x_5: *A, LF* (>80 µm) (less dense, i.e., density <1 g cm^{-3}, fraction with particles >80 µm), and x_6: *A, LF* (<80 µm) (less dense fraction passing through an 80 µm sieve). The seventh pool x_7 represents the dynamics of the *mineral associated* fraction (density >1 g cm^{-3}).

We also estimated the expected value of $\Delta^{14}C$ for the remaining years and these values can be seen in Figures S2 and S3 in Supporting Information S1.

The set of ordinary differential equations for the HFS model can be expressed in compartmental form as:

$$\begin{pmatrix} \dot{x}_1 \\ \dot{x}_2 \\ \dot{x}_3 \\ \dot{x}_4 \\ \dot{x}_5 \\ \dot{x}_6 \\ \dot{x}_7 \end{pmatrix} = \begin{pmatrix} 255 \\ 150 \\ 0 \\ 0 \\ 0 \\ 0 \\ 0 \end{pmatrix} + \begin{pmatrix} -255/1530 & 0 & 0 & 0 & 0 & 0 & 0 \\ 0 & -150/220 & 0 & 0 & 0 & 0 & 0 \\ 0 & 98/220 & -98/388 & 0 & 0 & 0 & 0 \\ 35/1530 & 0 & 4/388 & -39/1366 & 0 & 0 & 0 \\ 30/1530 & 0 & 0 & 0 & -30/90 & 0 & 0 \\ 0 & 0 & 0 & 0 & 24/90 & -24/1800 & 0 \\ 0 & 2.7/220 & 0 & 0 & 0 & 2.4/1800 & -5.1/560 \end{pmatrix} \begin{pmatrix} x_1 \\ x_2 \\ x_3 \\ x_4 \\ x_5 \\ x_6 \\ x_7 \end{pmatrix}. \quad (13)$$

3.3. Set of Parameters

As described before, in order to estimate the radiocarbon distributions and expected values of $\Delta^{14}C$, the algorithm needs the following arguments: a compartmental matrix **B**, containing the decomposition and transfer rates within the pools; an input vector ***u*** containing the input mass to be partitioned among the compartments; the year of observation (equivalent to year of sampling in an experimental framework); the number of years in the past one aims to compute the distributions for; and a set of radiocarbon values in the atmosphere, comprising the year of observation and the number of years chosen. An additional argument is h, the discretization size described above, which has a default value of 0.1 yr, but could be modified according to user preferences.

For the HFS model, **B** is the matrix in Equation 13, with the form of Equation 2, and ***u*** is the numeric vector in the same Equation 13, with similar form as Equation 3. We estimated the radiocarbon distributions for different years of observation, in order to address different research questions raised in this work. In the results and Appendix A, we present the distributions for the pools and total outflux of all the three models for the years 1965, 2027, and 2100. Additionally, in the supporting material we provide the non-stacked radiocarbon distributions of individual pools for the same mentioned years (Figures S4–S12 in Supporting Information S1), as well as the radiocarbon distributions for the total outflux and whole system for all the years between 1955 and 2100 (Videos S1–S6, respectively). Radiocarbon distributions of the outflux in the HFS model are also presented for the years 1996, 1998, 2002, and 2008, as for those years we also have independent $\Delta^{14}C$ data from soil CO_2 efflux in the Harvard Forest to compare to our estimations (Sierra, Trumbore, et al., 2012). For all those estimations, the number of years of computation was 1,000 yr. The bin size b for plotting the histograms was set as 10‰ for most of the radiocarbon distributions, except for the year 1965, where it was set up to 40‰, avoiding gaps on the x-axis.

3.3.1. Atmospheric Radiocarbon Data Sets

For the models studied here, we needed to build two different combinations of atmospheric radiocarbon curves. One for the Northern Hemisphere (NH) to cover the HFS and Emanuel models, and the second one for the tropics to serve as input for the Porce model (Figure 3).

The atmospheric $\Delta^{14}C$ values used for years in the past—for example, CE 1965—were obtained by merging the recently released IntCal20 calibration curve (Reimer et al., 2020), which combines radiocarbon data and Bayesian statistical interpolation for the range 55,000–0 cal BP (BP = *before present* = CE 1950), and the records of atmospheric radiocarbon data compiled by Graven et al. (2017), from CE 1950–2015 for the NH and for the tropics. Graven et al. (2017) also provide radiocarbon data in one-year resolution on the range 1850–1949. However, as in this range, there are estimations partially based on the previous NH calibration curve (IntCal13, Reimer et al., 2013), we decided to subset Graven et al. (2017)'s data set, starting in CE 1950.

For the years in the future, such as CE 2027 and CE 2100, we made use of the forecast simulations computed by Graven (2015), who simulated $\Delta^{14}C$ values in the atmosphere for four Representative Concentration Pathways of fossil fuel emissions: RCP2.6, RCP4.5, RCP6, and RCP8.5. In this work, we use the predictions based on the high emissions scenario (RCP8.5), starting in CE 2016.

The $\Delta^{14}C$ values in all data sets used in this work are written as the deviation from the standard representing the pre-industrial atmospheric ^{14}C concentration. The raw published values are already corrected for fractionation and decay with respect to the standard. It is equivalent to Δ in Stuiver and Polach (1977) (Equation 9).

4. Results

4.1. Shape of the Radiocarbon Distributions and Their Change Over Time

Overall, our results show that even though the age and transit time distributions for the compartmental systems at steady-state are static (Figures 4a, 5a, A2a, A3a, A5a, and A6a), the radiocarbon distributions are highly dynamic and non-normal (e.g., Figures 4b–4d, A2b–A2d, A5b–A5d, Videos S1–S6). They change dramatically over time as the atmospheric CO_2 source is affected by the bomb spike and the Suess effect (Suess, 1955), that is, the effect of the dilution of radiocarbon in the atmosphere due to the emission of fossil fuels (^{14}C-free). Pools that cycle fast, that is, pools with sharp age distribution peaks, such as *dead roots* and *Oi* in the HFS model or *foliage* in the

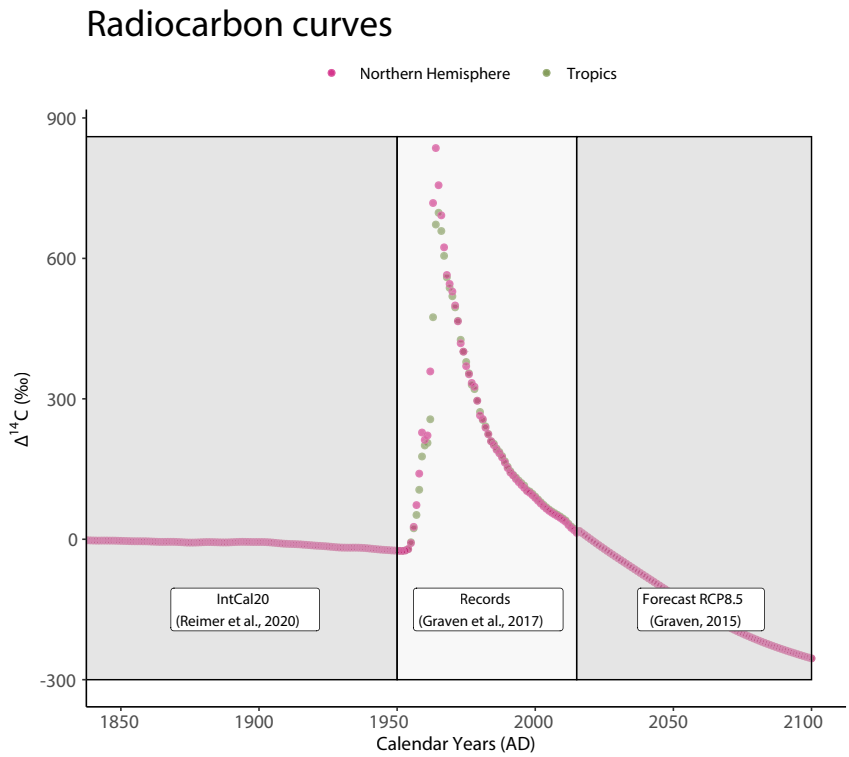

Figure 3. Scheme of the atmospheric radiocarbon inputs used in the estimation of the probability density distributions of radiocarbon. Before CE 1950, input radiocarbon data relies on the IntCal20 (Reimer et al., 2020) measurements and modeling; Between 1950 and 2015 it consists of atmospheric $\Delta^{14}CO_2$ records compiled by Graven et al. (2017); From 2016 on, the atmospheric radiocarbon values are based on the predictions of Graven (2015) for the RCP8.5 scenario. The records between 1950 and 2015 comprise values for the atmosphere in Northern Hemisphere (NH) and Tropics. The Tropics records are used as input in the Porce model (Appendix A1). The NH data set is used as input in the HFS model and Emanuel model (Appendix A2).

Porce model, followed most closely the radiocarbon dynamics in the atmosphere, while pools that cycle slowly showed a wide range of values. Consequently, the expected $\Delta^{14}C$ values also vary largely.

The distributions we obtained for the compartments of all models show very unique shapes for different years and the $\Delta^{14}C$ values are not normally distributed. In 1965, just after the peak of excess ^{14}C in the atmosphere due to nuclear weapon tests, pools that cycle fast had a wide $\Delta^{14}C$ range with high probability, due to the incorporation of radiocarbon values that changed rapidly over the period CE 1955–1964. Compartments that cycle slowly have a narrower distribution with their modes corresponding to negative $\Delta^{14}C$ values, as they represent pre-bomb atmospheric signals that varied less.

In the HFS model, for the whole system in CE 1965 (Figures 4b and S4 in Supporting Information S1), the distribution of radiocarbon aggregates the contributions of the different pools, which results in different peaks in the overall distribution. The mode (i.e., the $\Delta^{14}C$ with highest mass density) is below 0‰ because a large portion of the total amount of carbon is contributed by the *mineral associated* pool that is predominantly still pre-bomb carbon with little contribution from carbon fixed after 1964. In addition, other pools that cycle fast, contribute relatively small amounts of bomb ^{14}C to the overall distribution.

The radiocarbon distribution in the output flux of the HFS model in 1965, that is, the radiocarbon distribution that corresponds to the transit time distribution for this year (Figures 5b—blue bars—and S4 in Supporting Information S1) has three distinct peaks in the distribution. In the soil model, the distribution of the outflux is very similar to that of the *dead roots* pool (Figure S4 in Supporting Information S1), which is the main contributor to the total respiration flux. However, other pools also contribute to the respiration flux with their radiocarbon

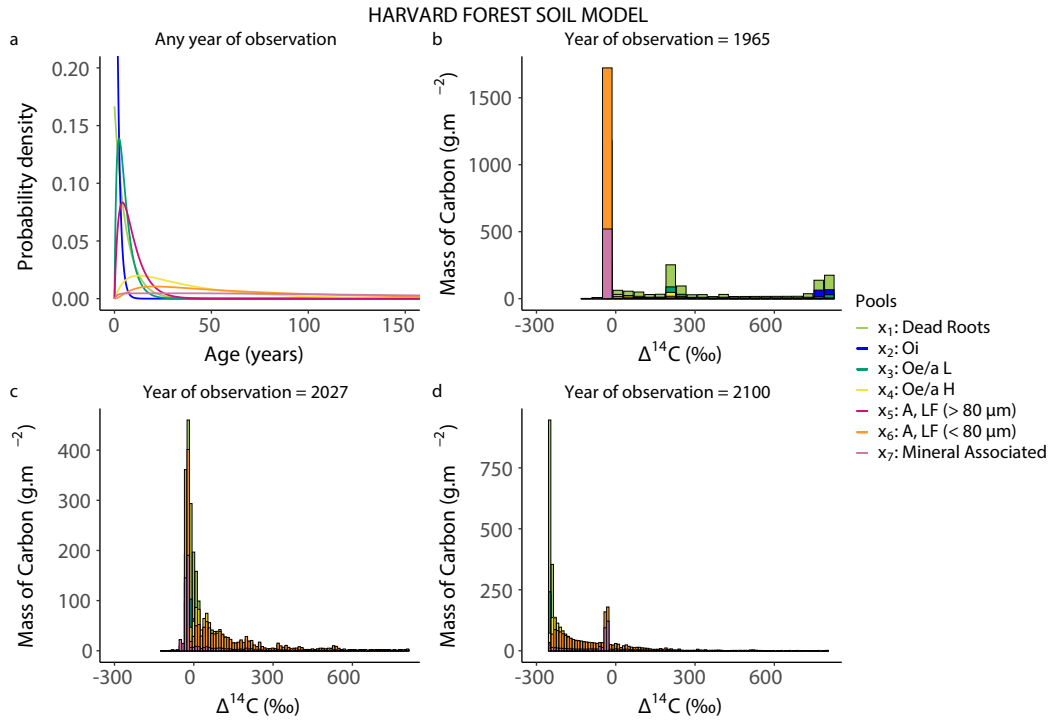

Figure 4. (a) Pool age distributions for the Harvard Forest Soil model computed in a span of 1,000 yr with a resolution of 0.1 yr. Mean system age is 50.9 yr. Mean pool ages vary from 1.5 yr (for *Oi* pool) to 150 yr (for *mineral associated* pool). (b) Mass density distribution of radiocarbon in 1965—just after the ^{14}C bomb peak in 1964. Distribution was computed over 1,000 yr, discretized by 0.1 yr. Bin size $b = 40‰$. The expected $\Delta^{14}C$ and standard deviation (sd) of the whole system in 1965 is $141 \pm 280‰$. (c) Mass density distribution of radiocarbon in 2027. Distribution was computed over 1,000 yr, discretized by 0.1 yr. Bin size $b = 10‰$. The expected $\Delta^{14}C$ and sd of the whole system in 2027 is $54 \pm 144‰$. (d) Mass density distribution of radiocarbon in 2100. Distribution was computed over 1,000 yr, discretized by 0.1 yr. Bin size $b = 10‰$. The expected $\Delta^{14}C$ and sd of the whole system in 2100 is $-147 \pm 146‰$.

signatures and emphasize fluxes from the fastest cycling pool (*Oi*) and respiration of carbon that was present in other pools before the bomb peak.

The shapes of the distributions change dramatically for subsequent years after the bomb spike (Figure 5b). For CE 2027, the expected $\Delta^{14}C$ values of fast pools drop considerably, in parallel with atmospheric ^{14}C, compared to CE 1965 (Figure S5 in Supporting Information S1). These fast pools do not store much radiocarbon from the bomb period, and their radiocarbon signatures reflect recent carbon from the atmosphere. In contrast, slow cycling pools in 2027 had relatively high $\Delta^{14}C$ values, mostly because they still contain radiocarbon from the bomb period. In the output flux (Figures 5b—green bars—and S5 in Supporting Information S1), as expected, since the respiration flux is dominated by the faster-cycling pools such as *dead roots* and *Oi* for HFS model, most of the radiocarbon is narrowly distributed around the recent atmospheric $\Delta^{14}CO_2$ value in 2027 ($\Delta^{14}CO_2 = -28.8‰$) (Graven, 2015), with almost no contributions from bomb ^{14}C.

By the year 2100, the atmospheric $\Delta^{14}CO_2$ values have dropped to $-254.5‰$ (Graven, 2015), reflecting the Suess effect. In all the models studied here, the distributions of most pools show a lower $\Delta^{14}C$ variability in 2100. Faster-cycling pools have dropped to reflect negative $\Delta^{14}C$ in the atmosphere over the 73 yr since 2027, while the slow pools still show a wide range of $\Delta^{14}C$ values that includes C fixed during the bomb period (now ~150 yr previously). The latter pattern can be observed for *mineral associated* (x_7), *A, LF* (<80 µm) (x_6) and *Oe/a H* (x_4) pools in the HFS model (Figure S6 in Supporting Information S1).

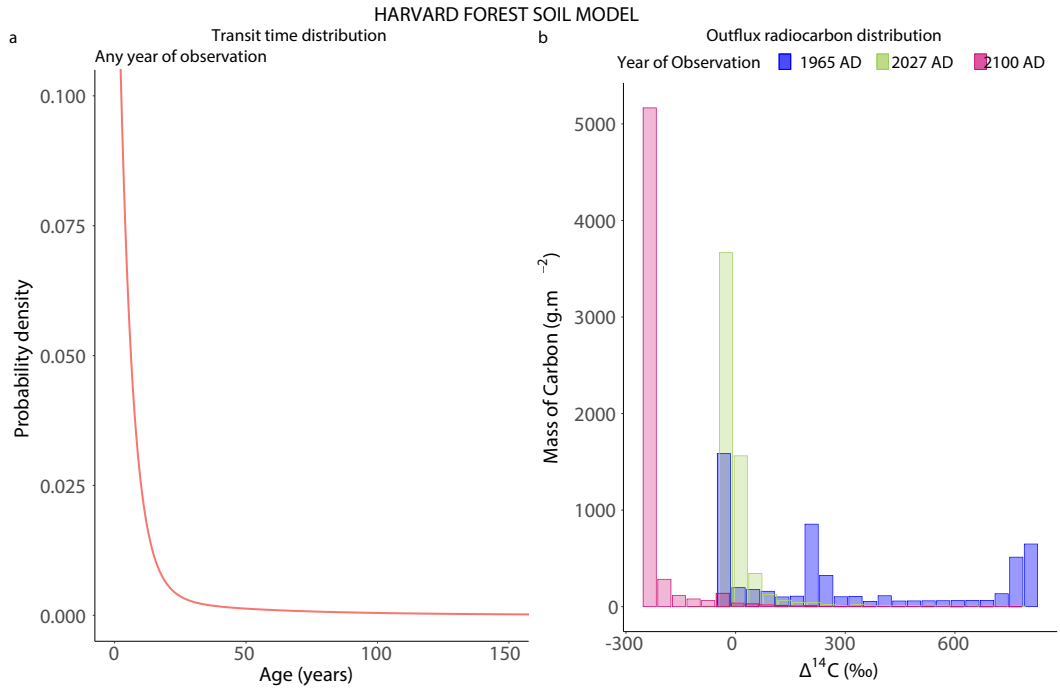

Figure 5. (a) Transit time distribution for the Harvard Forest Soil model computed in a span of 1,000 yr with a resolution of 0.1 yr. Mean transit time is 14.7 yr. (b) Mass density distributions of radiocarbon for the output flux (total respiration) in the years 1965, 2027, and 2100. Distribution was computed over 1,000 yr, discretized by 0.1 yr. Bin size b equals 40‰ for all the years of observation. The expected $\Delta^{14}C$ values and standard deviations of the outflux are: 334 ± 333‰ in 1965; 9 ± 81‰ in 2027; and −223 ± 78‰ in 2100.

4.2. Comparison With Measured Data

Radiocarbon measurements of total soil CO_2 efflux at the Harvard Forest compared relatively well with the theoretical distributions of radiocarbon in the output flux obtained from our approach. Total soil CO_2 efflux includes both decomposition sources predicted by the model and root respiration, estimated by Gaudinski et al. (2000) to be ∼55% and to have $\Delta^{14}C$ values equal to the atmosphere in any given year.

In the model, for all the years presented in this section (1996, 1998, 2002, and 2008) the mode represents a mass of respired carbon equivalent to $\sim 10^3$ gC m^{-2}. We refer also to smaller peaks, hereafter secondary peaks, where the mass of respired carbon is equivalent to values larger than 100 gC m^{-2} but lower than 1 kgC m^{-2} in one bin size (b) range. For all the theoretical distributions in this section b = 10‰, however, as one could anticipate, the size of the b has not effect on the expected value. The measurements were always within the expected range of $\Delta^{14}C$ estimated through the algorithm (Figure 6, Table 1). In all cases, the average of the measurements was relatively close to the expected value of the theoretical distributions. However, the variance of the observations was smaller than the expected variance from the model (Figure S3 in Supporting Information S1 and Video S7). In particular, the expected values were systematically higher in ^{14}C than the average of the observations for years 1996, 1998, 2002, and 2008 by 23.5‰, 21.8‰, 15.1‰, and 10.8‰, respectively (Figure 6). The sd of the observations were 17.3‰, 26.2‰, 8.4‰, and 13.6‰ for the years 1996, 1998, 2002, and 2008, respectively, which are smaller than the expected sd of the distributions, which were 107.6‰, 103.3‰, 96.3‰, and 89.7‰ for the corresponding years, as a consequence of the larger spread of the theoretical distributions.

For the year 1996 (Figure 6a), the 12 measurements of soil CO_2 efflux ranged from 104.3‰ to 167.3‰ (σ = 17.3‰). The mode of the theoretical distribution also falls in this interval: (112, 122]‰. Secondary peaks fall in a range with magnitude of one bin size below 0‰, starting in $\Delta^{14}C$ values of −28‰ and in a wide range of $\Delta^{14}C$ above the mode, ranging from 122‰ to 212‰ (Table 1).

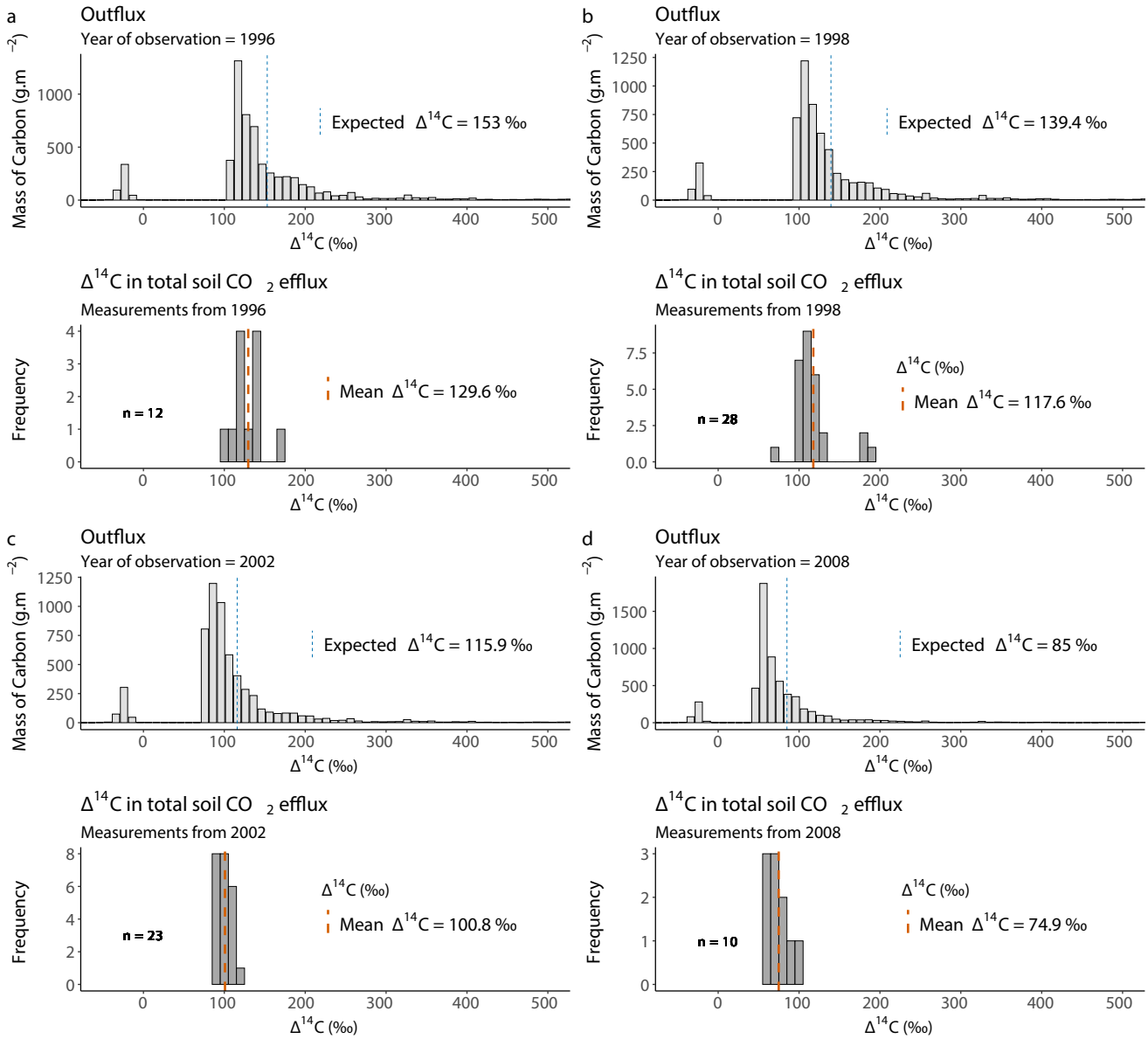

Figure 6. Comparison between theoretical radiocarbon distribution and independent empirical data for the corresponding years of observation. (a) Year of observation = CE 1996 = year of sampling and number of observations $n = 12$; (b) year of observation = CE 1998 = year of sampling and number of observations $n = 28$; (c) year of observation = CE 2002 = year of sampling and number of observations $n = 23$; (d) year of observation = CE 2008 = year of sampling and number of observations $n = 10$.

For the year 1998 (Figure 6b), the 28 measurements of soil CO_2 efflux ranged from 66.4‰ to 193.9‰, ($\sigma = 26.2$‰). The mode of the theoretical estimation fall in the range from 102‰ to 112‰ (Table 1), while secondary peaks are observed in the ranges (−28, −18], (92,102], and (112, 202].

For the year 2002 (Figure 6c), the 23 measurements of soil CO_2 efflux range from 88‰ to 117.9‰, ($\sigma = 8.4$‰). The theoretical mode falls partially in the range of the observations: (81, 101]‰. The theoretical estimations include the range observed in the empirical data – (102, 152]‰—however, with probability density one order of magnitude smaller than the mode. Moreover, the theoretical distribution has a secondary peak in the range of (71, 81], which is not observed in the measurements.

Table 1
$\Delta^{14}C$ Ranges With Masses of Carbon Above 100 gC m^{-2} According to Our Estimations; $\Delta^{14}C$ Expected Values According to Weighted Mean of Mass Distribution of Radiocarbon; and Observed $\Delta^{14}C$ Mean Values of Soil CO_2 Efflux

	$\Delta^{14}C$ [‰]			
Year	Mode[a]	Secondary peaks[b]	Expected value[c]	Mean value[d]
1996	(112, 122]	(−28, −18], (102, 112], (122, 212]	153 ± 107.6	129.5 ± 17.3
1998	(102, 112]	(−28, −18], (92, 102], (112, 202]	139.4 ± 103.3	117.6 ± 26.2
2002	(81, 101]	(−29, −19], (71, 81], (101, 151]	115.9 ± 96.3	100.8 ± 8.4
2008	(51, 61]	(-29, −19], (41, 51], (61, 121]	85 ± 89.7	74.8 ± 13.6

[a]Carbon masses $\sim 10^3$ gC m^{-2}. [b]Carbon masses between 100 gC m^{-2} and 1 kgC $^{-2}$. [c]Expected value of theoretical radiocarbon distribution of the outflux (weighted mean). [d]Mean value of the $\Delta^{14}C$ values measured on soil CO_2 efflux from the Harvard Forest.

Finally, in the year 2008 (Figure 6d), the 10 measurements of soil CO_2 efflux range from 60.8‰ to 104.7‰, ($\sigma = 13.6$‰). The peaks (carbon masses over 100 gC m^{-2}) of the theoretical distributions for this year are concentrated in the range (41, 121], with the mode in the bin (51, 61]‰.

For all the years, secondary peaks falling in the negative part of the $\Delta^{14}C$ axis (Table 1), comprising values between −29 or −28‰ and −19 or −18‰, are not captured in the soil $\Delta^{14}CO_2$ efflux measurements.

5. Discussion

5.1. How Do Distributions of Radiocarbon Change Over Time as a Consequence of Changes in Atmospheric Radiocarbon?

Our results clearly showed that distributions of radiocarbon in a compartmental system at steady-state change considerably over time, despite the stationarity of the age and transit time distributions for such systems, where the total mass of carbon does not change over time. These changes reflect recent and expected dramatic changes in the carbon isotopic signature of the inputs originating in the atmosphere, including the bomb spike and the Suess effect, which acts as tracer of the global carbon cycle.

In the non-steady-state case, the age and transit time distributions become also time-dependent. There are methods for obtaining age distributions of carbon in compartmental systems out of equilibrium (Metzler et al., 2018), however, the additional complexity that would be incorporated to the algorithm is outside the scope of this manuscript. We expect, nevertheless, that the topic of radiocarbon distributions for nonlinear and non-autonomous systems can be discussed in future work.

For fast cycling pools, we expect changes to match that of the radiocarbon content in the atmosphere. Consequently, the radiocarbon distributions for fast cycling pools present peaks in $\Delta^{14}C$ values similar to those from the contemporary atmospheric radiocarbon. That is an effect of the fast response of highly dynamic pools to the variations in the isotopic composition of the system inputs. As fast pools are the major contributors to the output flux, the total respiration also has similar narrow distributions close to the atmospheric $\Delta^{14}C$ in the year of observation t_0. For slow cycling pools that receive carbon from other pools, we expect wider distributions that include contributions from C fixed decades to centuries in the past. Thus, excess ^{14}C takes a longer time to be observed in the radiocarbon distributions of slow cycling pools.

As a consequence of fossil fuel (^{14}C-free) emissions to the atmosphere, the dilution of atmospheric radiocarbon (Suess effect, Suess, 1955) affects radiocarbon distributions, without affecting, however, the dynamic equilibrium (steady-state) of the compartmental system. This further widens distributions in slow cycling pools, and causes fast cycling pools to have lower $\Delta^{14}C$ values than slow cycling pools. The Suess effect becomes particularly relevant in the distributions for future years, as shown in the distributions of radiocarbon based on the forecast of atmospheric $\Delta^{14}CO_2$ values. The $\Delta^{14}CO_2$ in the atmosphere is estimated to achieve values as low as ca. −254‰ in 2100 for the RCP8.5 scenario (Graven, 2015). Such low values can emerge in the radiocarbon distributions of the pools with relatively high density in two cases: (a) if the pool cycles fast but the $\Delta^{14}C$ values in the atmos-

phere present high dilution (as in 2100), or (b) with natural or bomb, however non-diluted, $\Delta^{14}C$ values in the atmosphere, but in very slow cycling pools (i.e., >2,500 yr of carbon age). The latter case reflects sufficient time for radioactive decay to reduce radiocarbon ratios in the carbon residing in the system. In experiments, this could result in an inability to distinguish faster and slower cycling pools using $\Delta^{14}C$ average values. Thus, one advantage of using these radiocarbon distributions is to get insight into the dynamics of transfers in the compartmental system, highlighting when these become less meaningful in the future years. Such issues can begin as soon as in 2027, when the atmospheric $\Delta^{14}CO_2$ values start to decline to values never observed before by natural processes (i.e., without the anthropogenic effects such as the fossil fuel emissions). In the forecast for central Europe (Sierra, 2018), this transition year occurs as soon as 2022. This underlines the urgency of measurements in the current situation and the use of archived samples from the last decades, to emphasize the difference between fast pools that will track the changing atmosphere and slower pools that adjust more gradually and retain bomb ^{14}C signals even in future decades.

5.2. How Do Empirical Data Compare to These Conceptual Radiocarbon Distributions?

Measurements of radiocarbon in the output flux of a soil system suggest that field measurements capture the mean value of the distributions, but not necessarily the variance of its distribution. The observations tend to be around the mean value with a fairly small sd. Conversely, the estimate of $\Delta^{14}C$ values from the model show that for slow cycling pools, the spread of the $\Delta^{14}C$ distributions can capture almost all the atmospheric $\Delta^{14}CO_2$ history.

Although we do not have independent observations available for specific pools to compare with our model predictions, we expect that for fast cycling pools the measurements will fall in a narrow range of $\Delta^{14}C$ values, as can be observed in experiments assessing the fossil fuel CO_2 distribution by measurements of $\Delta^{14}C$ on deciduous leaves (Santos et al., 2019). For slow cycling pools, we would expect that the variability of $\Delta^{14}C$ experimental data will be broader.

Carbon pools that cycle slowly can be very important for climate change mitigation, since they could store carbon for a longer time. Therefore, an accurate understanding of their dynamics is crucial. A valuable tool to assess these dynamics is using radiocarbon as a tracer to further constrain models. However, based on our results and interpretations, we believe that future research work should attempt at better capturing the spread of radiocarbon values in such pools.

We recognize that the variability in the observations includes measurement uncertainty in addition to the expected variability due to the age distribution of carbon and the atmospheric radiocarbon history. Nevertheless, the comparison of the variability between measurements and the theoretical distributions help to contextualize the origin of the observed variance and interpret measurements performed in different years.

5.3. What Insights Can These Distributions Provide for Experimental and Sampling Design for Improving Model-Data Comparisons by Capturing the Entire Variability of $\Delta^{14}C$ Values?

Overall, our results have implications for the interpretation of measured radiocarbon data. The radiocarbon distributions computed here can also give useful insights for the design of empirical studies. The number of samples required to adequately represent the internal variability in radiocarbon depends on the year of observation and the particular compartment of interest. Our results suggest that fast cycling pools can have their $\Delta^{14}C$ mean determined with a low sample size. For example, this would be the case for *dead roots* and *Oi* pools in the HFS model; *foliage* and *fine litter* in the Porce model; and *non-woody tree parts* and *ground vegetation* in the Emanuel model. A priori, determining exact sample sizes may be a suitable approach for future studies. For samples already collected, caution must be taken in interpreting the results, since a bulk measurement may not capture the whole distribution of possible radiocarbon values.

Our study opens up new opportunities to empirically determining radiocarbon distributions in compartmental systems. For example, this could be achieved by sampling designs that are representative of the compartments with higher variance, making sure the number of samples catches the entire potential variability. This way, it should be possible to determine empirical radiocarbon distributions. Consequently, empirical determination of

radiocarbon distributions in compartmental systems could be used to obtain age and transit time distributions using inverse statistical methods. This offers tremendous opportunities for accurate estimations of time metrics, incorporating the complexity of biological systems through multiple interconnected compartments. However, more research is still needed to determine whether radiocarbon distributions map to unique age and transit time distributions. To guarantee the uniqueness of the age and transit time distributions from compartmental systems, one should be able to assure that only one combination of rates in the compartmental matrix builds the estimated distributions.

Moreover, as pointed out by Gaudinski et al. (2000), limited information about the cycling rates are obtained by ^{14}C measurements of bulk SOM made at a single point in time. Therefore, being able to compute radiocarbon distributions for different years of observation could improve the interpretations of the time-evolution of carbon in compartmental systems.

6. Conclusion

We introduced here a new method to obtain probability distributions of radiocarbon in open compartmental systems based on previous knowledge on the age distribution of carbon and the time history of atmospheric $\Delta^{14}CO_2$. By applying this method to different models, we were able to infer potential shapes of radiocarbon distributions in compartments that strongly change over time and depend on how fast carbon cycles within each compartment.

Radiocarbon distributions (formally distributions of $\Delta^{14}C$) cannot be interpreted directly as distributions of age of carbon. Distinctively to age, $\Delta^{14}C$ values in a pool do not increase/decrease monotonically; in addition, the $\Delta^{14}C$ mean value changes over time due to inputs from the atmospheric signal and mixing inside and among compartments even for systems at steady-state—in contrast to age distributions, which do not change with the year of observation for such systems. This implies that we can have two or more different calendar years with the same $\Delta^{14}C$. Therefore, despite age and transit time distributions for systems in steady-state being static, radiocarbon distributions' shape, expected value, mode, and variance are expected to vary greatly over time, especially since the beginning of the Anthropocene epoch.

Radiocarbon distributions can be used together with the known changes in atmospheric $\Delta^{14}CO_2$ to evaluate how models predict the changing distributions of radiocarbon in each compartment and its output over the last decades. This provides a reliable and consistent method to test models against observations of systems in equilibrium and to refine model representations of C dynamics in soils and ecosystems.

Appendix A: Additional Study Cases

In this work, we also computed the radiocarbon distributions for two additional compartmental models. One model represents the carbon cycle of an old-growth tropical forest ecosystem based on measurements made at the Porce region in Colombia. The model parameters were obtained through a data assimilation procedure on the empirical data. We denote it here as the Porce model (Sierra et al., 2021). Another model represents the global carbon cycle, and it is based on the simple model described by Emanuel et al. (1981). We refer to it here as the Emanuel model.

A1. Porce Model

The Porce model consists of seven compartments representing x_1: *Foliage*, x_2: *Wood*, x_3: *Fine roots*, x_4: *Coarse roots*, x_5: *Fine litter*, x_6: *Coarse woody debris*, and x_7: *Soil carbon* (0–30 cm). Carbon enters the *foliage* compartment in the form of gross primary production, with an average value of 23.7 MgC ha^{-1} yr^{-1}. From the *foliage* (x_1), carbon is transferred to the *wood* and root pools (x_2, x_3, x_4), and from these live biomass pools, carbon is subsequently transferred to the dead biomass and soil pools (x_5, x_6, x_7). A pictorial structure of this compartmental system can be visualized on Figure A1. In compartmental form, the Porce model can be expressed as Equation A1.

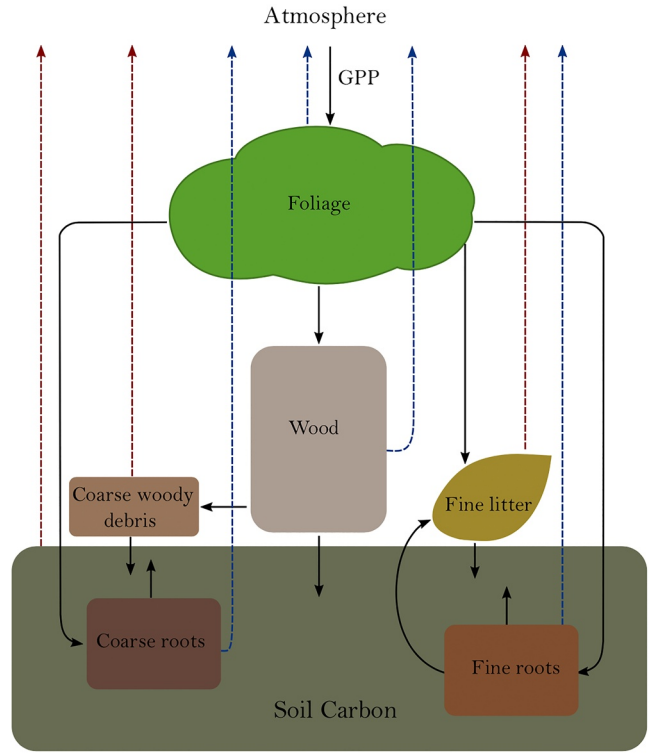

Figure A1. Scheme representing the connection between compartments in Porce model (Sierra et al., 2021). The pools are identified as x_1: *Foliage*, x_2: *Wood*, x_3: *Fine roots*, x_4: *Coarse roots*, x_5: *Fine litter*, x_6: *Coarse woody debris*, and x_7: *Soil carbon* (0–30 cm). Pools x_1–x_4 are live biomass pools, while dead biomass and soil pools correspond to compartments x_5, x_6, and x_7.

$$\begin{pmatrix} \dot{x}_1 \\ \dot{x}_2 \\ \dot{x}_3 \\ \dot{x}_4 \\ \dot{x}_5 \\ \dot{x}_6 \\ \dot{x}_7 \end{pmatrix} = \begin{pmatrix} 23.74 \\ 0 \\ 0 \\ 0 \\ 0 \\ 0 \\ 0 \end{pmatrix} + \begin{pmatrix} -2.98 & 0 & 0 & 0 & 0 & 0 & 0 \\ 0.47 & -0.03 & 0 & 0 & 0 & 0 & 0 \\ 0.03 & 0 & -0.03 & 0 & 0 & 0 & 0 \\ 0.09 & 0 & 0 & -0.02 & 0 & 0 & 0 \\ 0.75 & 0 & 0.03 & 0 & -2.6 & 0 & 0 \\ 0 & 0.009 & 0 & 0.00002 & 0 & -0.52 & 0 \\ 0 & 0 & 0 & 0 & 0.66 & 0.51 & -0.02 \end{pmatrix} \begin{pmatrix} x_1 \\ x_2 \\ x_3 \\ x_4 \\ x_5 \\ x_6 \\ x_7 \end{pmatrix}, \quad \text{(A1)}$$

The age and transit time distributions of this compartmental model can be observed in Figures A2a and A3a, respectively. Additionally, from the age and transit time distributions, we have also computed the radiocarbon distributions for the years 1965, 2027, and 2100 (Figures A2b–A2d, A3b, and S7–S9 in Supporting Information S1), as well as the radiocarbon distributions of the whole system and its total outflux for the period between 1955 and 2100 (Videos S3 and S4). The arguments of the functions used to compute the theoretical radiocarbon distributions are the same ones used for the HFS model, following Section 3.3. Therefore, the bin size b of the distributions for the year 1965 is $b = 40‰$, while for 2027 and 2100 it is set as $b = 10‰$.

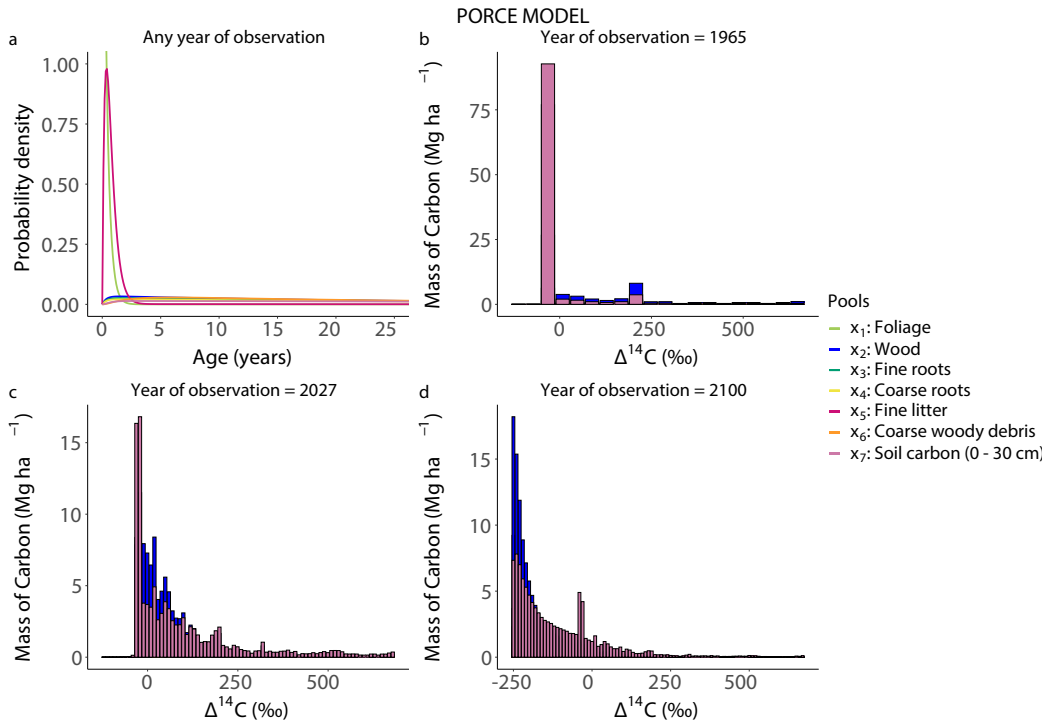

Figure A2. (a) Pool age distributions for the Porce model computed in a span of 1,000 yr with a resolution of 0.1 yr. Mean system age is 40.7 yr. Mean pool ages vary from 0.3 yr (for *foliage* pool) to 55.3 yr (for *soil carbon* pool). (b) Mass density distribution of radiocarbon for 1965—just after the ^{14}C bomb peak in 1964. Distribution was computed over 1,000 yr, discretized by 0.1 yr. Bin size $b = 40‰$. The expected $\Delta^{14}C$ and sd of the whole system in 1965 is $62.3 \pm 193‰$. (c) Mass density distribution of radiocarbon for 2027. Distribution was computed over 1,000 yr, discretized by 0.1 yr. Bin size $b = 10‰$. The expected $\Delta^{14}C$ and sd of the whole system in 2027 is $85.4 \pm 151‰$. (d) Mass density distribution of radiocarbon for 2100. Distribution was computed over 1,000 yr, discretized by 0.1 yr. Bin size $b = 10‰$. The expected $\Delta^{14}C$ and sd of the whole system in 2100 is $-147.9 \pm 131‰$.

As observed in the HFS model, the probability distribution of radiocarbon for the whole system has the mode on $\Delta^{14}C$ values of the main contributor, a slow cycling pool: *Soil carbon* (0–30 cm) (Figures A2b–A2d and S7–S9 in Supporting Information S1). Moreover, for the year 2100, where the atmospheric $\Delta^{14}CO_2$ will most likely have largely dropped due to the Suess effect (Graven, 2015), the distribution of radiocarbon of slow pools is wide.

In the outflux of the Porce model (Figures A3b and S7–S9 in Supporting Information S1), the peaks are related to the fast dynamics of pools, such as *foliage* and *fine litter*. The expected $\Delta^{14}C$ values in the year of observation of the fast pools will change according to the atmospheric radiocarbon signals detected for the contemporaneous years of sampling (Figures S7–S9 in Supporting Information S1).

A2. Emanuel Model

The Emanuel model was published in 1981 and consists of a 5-box model of the global terrestrial carbon cycle. The boxes represent the pools x_1: *Non-woody tree parts*, x_2: *Woody tree parts*, x_3: *Ground vegetation*, x_4: *Detritus/Decomposers*, and x_5: *Active soil carbon*. There are inputs from the atmosphere to two pools (x_1 and x_3). From x_1 carbon is partitioned into pools x_2 and x_4. Carbon from x_3 partition into pool x_5, which also receives the transfers from pools x_2 and x_4. All the stocks (in PgC) and transfers among the compartments (in PgC yr^{-1}) can be visualized in the scheme on Figure A4. In compartmental form, the Emanuel model is represented by Equation A2.

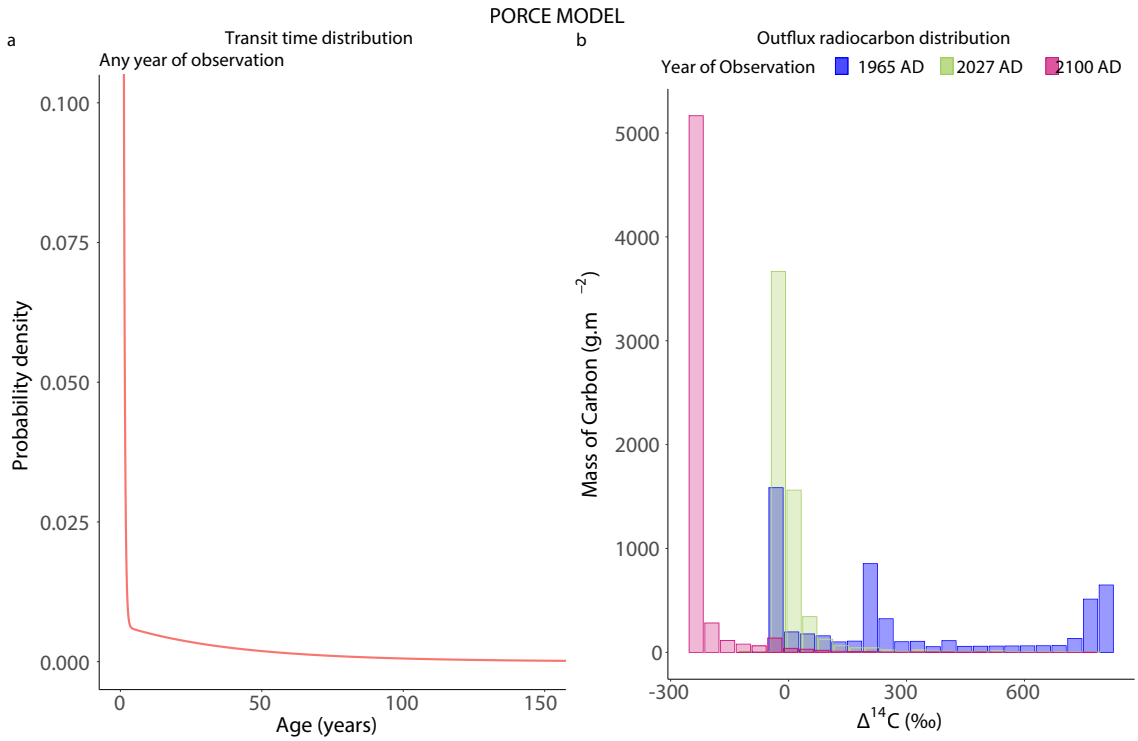

Figure A3. (a) Transit time distribution for the Porce model computed in a span of 1,000 yr with a resolution of 0.1 yr. Mean transit time is 11.3 yr. (b) Mass density distributions of radiocarbon for the output flux (total respiration) in the years 1965, 2027, and 2100. Distribution was computed over 1,000 yr, discretized by 0.1 yr. Bin size b equals 40‰ for all the years of observation. The expected $\Delta^{14}C$ values and standard deviations of the outflux are: 532 ± 292‰ in 1965; 1.1 ± 90‰ in 2027; and −227 ± 80‰ in 2100.

$$\begin{pmatrix} \dot{x}_1 \\ \dot{x}_2 \\ \dot{x}_3 \\ \dot{x}_4 \\ \dot{x}_5 \end{pmatrix} = \begin{pmatrix} 77 \\ 0 \\ 36 \\ 0 \\ 0 \end{pmatrix} + \begin{pmatrix} -77/37 & 0 & 0 & 0 & 0 \\ 31/37 & -31/452 & 0 & 0 & 0 \\ 0 & 0 & -36/69 & 0 & 0 \\ 21/37 & 15/452 & 12/69 & -48/81 & 0 \\ 0 & 2/452 & 6/69 & 3/81 & -11/1121 \end{pmatrix} \begin{pmatrix} x_1 \\ x_2 \\ x_3 \\ x_4 \\ x_5 \end{pmatrix}, \tag{A2}$$

As pointed out by Emanuel et al. (1981), the *active soil carbon* compartment x_5 has a turnover time much smaller than 1,000 yr. Therefore, the choice of *nyears* parameter equals to 1,000 yr is plausible and sufficient for the coverage of the entire variability in the computation. The radiocarbon data used to initialize the algorithm was the same used for the HFS model, discussed in Section 3.3.1. The arguments of the functions used to compute the theoretical radiocarbon distributions are the same ones used for the HFS and Porce models, following Section 3.3. Particularly for the aggregation step, it means the bin size b of the distributions for the year 1965 is $b = 40‰$, while for 2027 and 2100 it is set as $b = 10‰$.

The age and transit time distributions of this compartmental model can be observed in Figures A5a and A6a. Moreover, from the age and transit time distributions, we have also computed the radiocarbon distributions for the years 1965, 2027, and 2100 (Figures A5b–A5d, A6b, S10–S12 in Supporting Information S1), as well as the radiocarbon distributions of the whole system and its total outflux for the period between 1955 and 2100 (Videos S5 and S6).

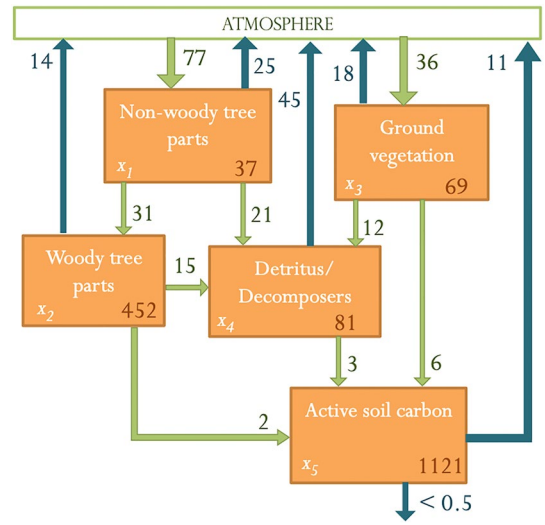

Figure A4. Scheme representing the stocks (in PgC) and fluxes (in PgC yr^{-1}) among compartments in Emanuel model (adapted from Emanuel et al., 1981). Pools are numbered as x_1: *Non-woody tree parts*, x_2: *Woody tree parts*, x_3: *Ground vegetation*, x_4: *Detritus/Decomposers*, and x_5: *Active soil carbon*.

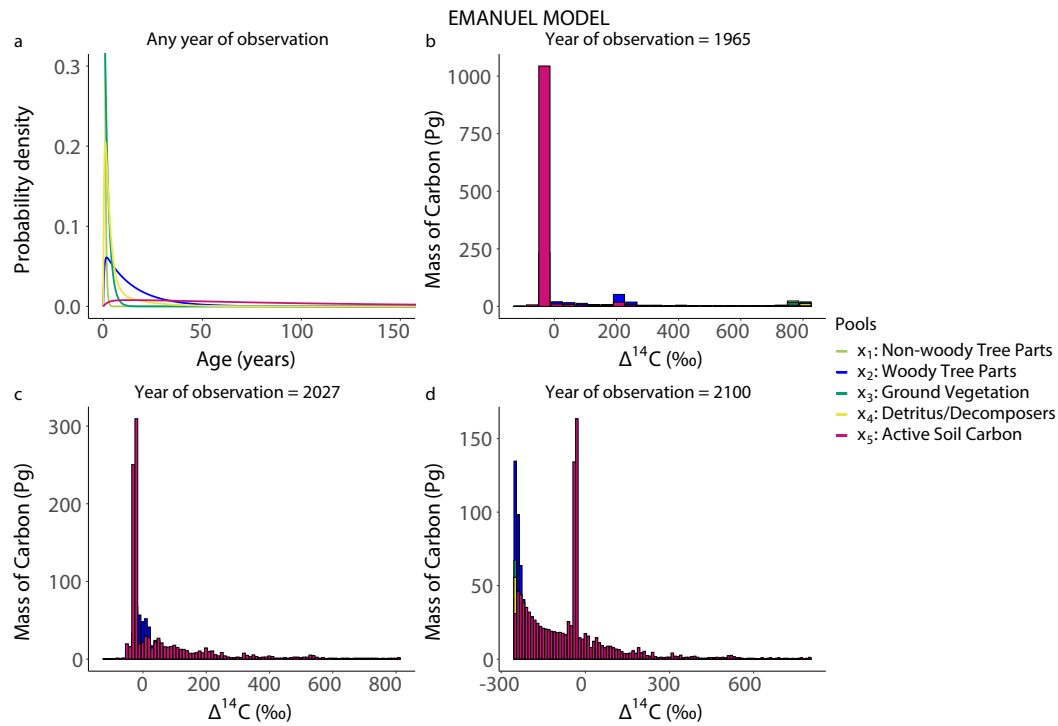

Figure A5. (a) Pool age distributions for the Emanuel model computed in a span of 1,000 yr with a resolution of 0.1 yr. Mean system age is 72.8 yr. Mean pool ages vary from 0.5 yr (for *non-woody tree parts* pool) to 108 yr (for *active soil carbon* pool). (b) Mass density distribution of radiocarbon for 1965—just after the ^{14}C bomb peak in 1964. Distribution was computed over 1,000 yr, discretized by 0.1 yr. Bin size $b = 40‰$. The expected $\Delta^{14}C$ and standard deviation (sd) of the whole system in 1965 is $98 \pm 255‰$. (c) Mass density distribution of radiocarbon for 2027. Distribution was computed over 1,000 yr, discretized by 0.1 yr. Bin size $b = 10‰$. The expected $\Delta^{14}C$ and sd of the whole system in 2027 is $53 \pm 146‰$. (d) Mass density distribution of radiocarbon for 2100. Distribution was computed over 1,000 yr, discretized by 0.1 yr. Bin size $b = 10‰$. The expected $\Delta^{14}C$ and sd of the whole system in 2100 is $-116 \pm 161‰$.

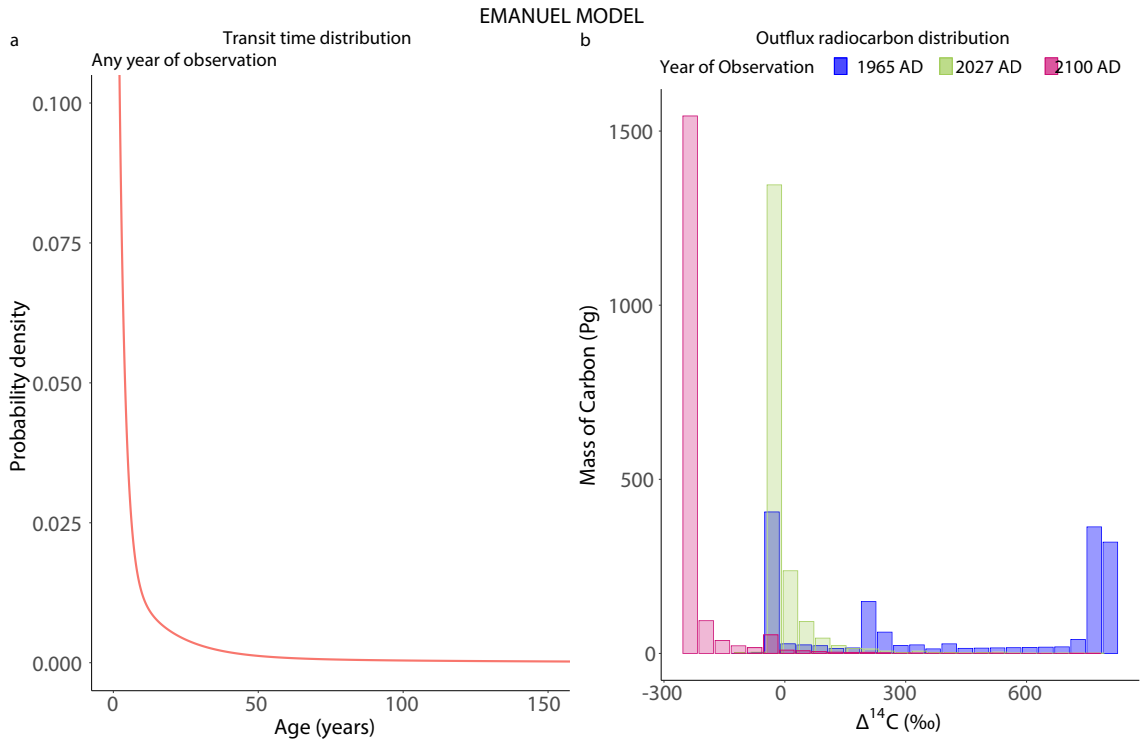

Figure A6. (a) Transit time distribution for the Emanuel model computed in a span of 1,000 yr with a resolution of 0.1 yr. Mean transit time is 15.6 yr. (b) Mass density distributions of radiocarbon for the output flux (total respiration) in the years 1965, 2027, and 2100. Distribution was computed over 1,000 yr, discretized by 0.1 yr. Bin size *b* equals 40‰ for all the years of observation. The expected $\Delta^{14}C$ values and standard deviations of the outflux are: 467 ± 354‰ in 1965; 2.2 ± 78‰ in 2027; and −225 ± 80‰ in 2100.

As observed for the other two models, slower pools also show a wider $\Delta^{14}C$ distribution in the Emanuel model. The widest distributions are from *woody tree parts* and *active soil carbon* (Figures S10–S12 in Supporting Information S1). This might reflect the slow incorporation of the input radiocarbon signal to those pools.

In the Emanuel model, the largest outflux back to atmosphere comes from the *detritus/decomposers* pool (45 PgC yr^{-1}; Figure A4). Analogously to the HFS model, the Emanuel model has its outflux radiocarbon distribution (Figure A6b) similar to the distributions of the fast cycling pools, such as *detritus/decomposers* (Figures S10–S12 in Supporting Information S1), however, the expected $\Delta^{14}C$ values are evidently different (Figures S10–S12 in Supporting Information S1).

Data Availability Statement

The atmospheric $\Delta^{14}CO_2$ data sets used in this research are available through Graven (2015), Graven et al. (2017), and Reimer et al. (2020) or http://intcal.org. Data on the compartmental model presented in this research as HFS model, including the independent $\Delta^{14}C$ data used for comparisons with our estimations are available through Sierra, Trumbore, et al. (2012). The coefficients used for the Porce model are available in Sierra et al. (2021). The global carbon cycle compartmental model used here, namely Emanuel model, can be accessed in Emanuel et al. (1981). The algorithm developed to estimate the radiocarbon distributions in the individual compartments, the whole system and the outflux, as well as an R script to plot the distributions and calculate the expected values of the distributions have been permanently archived in Zenodo with the digital object identifier https://doi.org/10.5281/zenodo.6373329 (Chanca, 2022).

Acknowledgments
The authors would like to thank Ingeborg Levin for the meaningful comments and suggestions on this work. This work is also stimulated by the scientific research developed at the Amazon Tall Tower Observatory (ATTO), which is partly funded by the German Federal Ministry of Education and Research (grant number 01LK1602A) and the Max Planck Society. Open access funding enabled and organized by Projekt DEAL.

References

Anderson, D. H. (1983). *Compartmental modeling and tracer kinetics* (Vol. 50). Springer Science & Business Media. https://doi.org/10.1007/978-3-642-51861-4

Azizi-Rad, M., Chanca, I., Herrera-Ramírez, D., Metzler, H., & Sierra, C. A. (2021). Stochastic and deterministic interpretation of pool models. *Global Change Biology*, *27*(11), 2271–2272. https://doi.org/10.1111/gcb.15581

Bolin, B., & Rodhe, H. (1973). A note on the concepts of age distribution and transit time in natural reservoirs. *Tellus*, *25*(1), 58–62. https://doi.org/10.3402/tellusa.v25i1.9644

Emanuel, W., Killough, G., & Olson, J. (1981). *Modeling the circulation of carbon in the world's terrestrial ecosystem, carbon cycle modeling, scope, 16 b. bolin* (pp. 335–353). John Wiley.

Gaudinski, J. B., Trumbore, S. E., Davidson, E. A., & Zheng, S. (2000). Soil carbon cycling in a temperate forest: Radiocarbon-based estimates of residence times, sequestration rates and partitioning of fluxes. *Biogeochemistry*, *51*(1), 33–69. https://doi.org/10.1023/a:1006301010014

Goudriaan, J. (1992). Biosphere structure, carbon sequestering potential, and the atmospheric ^{14}C carbon record. *Journal of Experimental Botany*, *43*(8), 1111–1119. https://doi.org/10.1093/jxb/43.8.1111

Graven, H. D. (2015). Impact of fossil fuel emissions on atmospheric radiocarbon and various applications of radiocarbon over this century. *Proceedings of the National Academy of Sciences*, *112*(31), 9542–9545. https://doi.org/10.1073/pnas.1504467112

Graven, H. D., Allison, C. E., Etheridge, D. M., Hammer, S., Keeling, R. F., & Levin, I. (2017). Compiled records of carbon isotopes in atmospheric CO_2 for historical simulations in CMIP6. *Geoscientific Model Development*, *10*(12), 4405–4417. https://doi.org/10.5194/gmd-10-4405-2017

Hogg, A. G., Heaton, T. J., Hua, Q., Palmer, J. G., Turney, C. S., Southon, J., et al. (2020). SHCal20 southern hemisphere calibration, 0–55,000 yr cal bp. *Radiocarbon*, *62*(4), 759–778. https://doi.org/10.1017/rdc.2020.59

Hogg, A. G., Hua, Q., Blackwell, P. G., Niu, M., Buck, C. E., Guilderson, T. P., et al. (2013). SHCal13 southern hemisphere calibration, 0–50,000 yr cal bp. *Radiocarbon*, *55*(4), 1889–1903. https://doi.org/10.2458/azu_js_rc.55.16783

Hua, Q., Barbetti, M., & Rakowski, A. Z. (2013). Atmospheric radiocarbon for the period 1950–2010. *Radiocarbon*, *55*(4), 2059–2072. https://doi.org/10.2458/azu_js_rc.v55i2.16177

Hua, Q., Turnbull, J. C., Santos, G. M., Rakowski, A. Z., Ancapichún, S., De Pol-Holz, R., et al. (2021). Atmospheric radiocarbon for the period 1950–2019. *Radiocarbon*, 1–23. https://doi.org/10.1017/rdc.2021.95

Jacquez, J. A., & Simon, C. P. (1993). Qualitative theory of compartmental systems. *SIAM Review*, *35*(1), 43–79. https://doi.org/10.1137/1035003

Jain, A. K., Kheshgi, H. S., & Wuebbles, D. J. (1997). Is there an imbalance in the global budget of bomb-produced radiocarbon? *Journal of Geophysical Research: Atmospheres*, *102*(D1), 1327–1333. https://doi.org/10.1029/96jd03092

Lawrence, C. R., Beem-Miller, J., Hoyt, A. M., Monroe, G., Sierra, C. A., Stoner, S. (2020). An open source database for the synthesis of soil radiocarbon data: International Soil Radiocarbon Database (ISRaD) version 1.0. *Earth System Science Data*, *12*, 61–76. https://doi.org/10.5194/essd-12-61-2020

Levin, I., & Kromer, B. (1997). Twenty years of atmospheric $^{14}CO_2$ observations at Schauinsland station, Germany. *Radiocarbon*, *39*(2), 205–218. https://doi.org/10.1017/s0033822200052012

Levin, I., Münnich, K., & Weiss, W. (1980). The effect of anthropogenic CO_2 and ^{14}C sources on the distribution of ^{14}C in the atmosphere. *Radiocarbon*, *22*(2), 379–391. https://doi.org/10.1017/s003382220000967x

Levin, I., Naegler, T., Kromer, B., Diehl, M., Francey, R., Gomez-Pelaez, A., & Worthy, D. (2010). Observations and modeling of the global distribution and long-term trend of atmospheric $^{14}CO_2$. *Tellus B: Chemical and Physical Meteorology*, *62*(1), 26–46. https://doi.org/10.1111/j.1600-0889.2009.00446.x

Metzler, H., Müller, M., & Sierra, C. A. (2018). Transit-time and age distributions for nonlinear time-dependent compartmental systems. *Proceedings of the National Academy of Sciences*, *115*(6), 1150–1155. https://doi.org/10.1073/pnas.1705296115

Metzler, H., & Sierra, C. A. (2018). Linear autonomous compartmental models as continuous-time Markov chains: Transit-time and age distributions. *Mathematical Geosciences*, *50*(1), 1–34. https://doi.org/10.1007/s11004-017-9690-1

Naegler, T., Ciais, P., Rodgers, K., & Levin, I. (2006). Excess radiocarbon constraints on air-sea gas exchange and the uptake of CO_2 by the oceans. *Geophysical Research Letters*, *33*(11). https://doi.org/10.1029/2005gl025408

Randerson, J., Enting, I., Schuur, E., Caldeira, K., & Fung, I. (2002). Seasonal and latitudinal variability of troposphere $\Delta^{14}CO_2$: Post bomb contributions from fossil fuels, oceans, the stratosphere, and the terrestrial biosphere. *Global Biogeochemical Cycles*, *16*(4), 59-1–59-19. https://doi.org/10.1029/2002gb001876

Rasmussen, M., Hastings, A., Smith, M. J., Agusto, F. B., Chen-Charpentier, B. M., & Hoffman, F. M. (2016). Transit times and mean ages for nonautonomous and autonomous compartmental systems. *Journal of Mathematical Biology*, *73*(6–7), 1379–1398. https://doi.org/10.1007/s00285-016-0990-8

Reimer, P. J., Austin, W. E., Bard, E., Bayliss, A., Blackwell, P. G., & Ramsey, C. B. (2020). The IntCal20 Northern Hemisphere radiocarbon age calibration curve (0–55 cal kbp). *Radiocarbon*, *62*(4), 725–757. https://doi.org/10.1017/rdc.2020.41

Reimer, P. J., Bard, E., Bayliss, A., Beck, J. W., Blackwell, P. G., & Ramsey, C. B. (2013). IntCal13 and Marine13 radiocarbon age calibration curves 0–50,000 yr cal bp. *Radiocarbon*, *55*(4), 1869–1887. https://doi.org/10.2458/azu_js_rc.55.16947

Santos, G. M., Oliveira, F. M., Park, J., Sena, A. C., Chiquetto, J. B., Macario, K. D., & Grainger, C. S. (2019). Assessment of the regional fossil fuel CO_2 distribution through $\Delta^{14}C$ patterns in ipê leaves: The case of Rio de Janeiro state, Brazil. *City and Environment Interactions*, *1*, 100001. https://doi.org/10.1016/j.cacint.2019.06.001

Sierra, C. A. (2018). Forecasting atmospheric radiocarbon decline to pre-bomb values. *Radiocarbon*, *60*(4), 1055–1066. https://doi.org/10.1017/rdc.2018.33

Sierra, C. A., Ceballos-Núñez, V., Metzler, H., & Müller, M. (2018). Representing and understanding the carbon cycle using the theory of compartmental dynamical systems. *Journal of Advances in Modeling Earth Systems*, *10*(8), 1729–1734. https://doi.org/10.1029/2018ms001360

Sierra, C. A., Estupinan-Suarez, L. M., & Chanca, I. (2021). The fate and transit time of carbon in a tropical forest. *Journal of Ecology*, *109*(8), 2845–2855. https://doi.org/10.1111/1365-2745.13723

Sierra, C. A., Müller, M., Metzler, H., Manzoni, S., & Trumbore, S. (2017). The muddle of ages, turnover, transit, and residence times in the carbon cycle. *Global Change Biology*, *23*(5), 1763–1773. https://doi.org/10.1111/gcb.13556

Sierra, C. A., Müller, M., Trumbore, S. (2012). Models of soil organic matter decomposition: The SoilR package, version 1.0. *Geoscientific Model Development*, *5*, 1045–1060. https://doi.org/10.5194/gmd-5-1045-2012

Sierra, C. A., Müller, M., & Trumbore, S. (2014). Modeling radiocarbon dynamics in soils: SoilR version 1.1. *Geoscientific Model Development*, *7*(5), 1919–1931. https://doi.org/10.5194/gmd-7-1919-2014

Sierra, C. A., Trumbore, S., Davidson, E., Frey, S., Savage, K., & Hopkins, F. (2012). Predicting decadal trends and transient responses of radiocarbon storage and fluxes in a temperate forest soil. *Biogeosciences*, *9*(8), 3013–3028. https://doi.org/10.5194/bg-9-3013-2012

Stuiver, M., & Polach, H. A. (1977). Discussion reporting of ^{14}C data. *Radiocarbon*, *19*(3), 355–363. https://doi.org/10.1017/s0033822200003672
Suess, H. E. (1955). Radiocarbon concentration in modern wood. *Science*, *122*(3166), 415–417. https://doi.org/10.1126/science.122.3166.415.b
Thompson, M. V., & Randerson, J. T. (1999). Impulse response functions of terrestrial carbon cycle models: Method and application. *Global Change Biology*, *5*(4), 371–394. https://doi.org/10.1046/j.1365-2486.1999.00235.x